Physica A 392 (2013) 4231–4241

Contents lists available at SciVerse ScienceDirect

Physica A

journal homepage: www.elsevier.com/locate/physa

Dynamical properties for a mixed Fermi accelerator model

Danila F. Tavares [a,b], A.D. Araujo [b], Edson D. Leonel [c], R.N. Costa Filho [b,*]

[a] Universidade da Integração Internacional da Lusofonia Afro-Brasileira - UNILAB, Campus da Liberdade Avenida da Abolição, 3 - Centro-Redenção - CE, Brazil

[b] Departamento de Física, Universidade Federal do Ceará, Caixa Postal 6030, Campus do Pici, 60455-760 Fortaleza, Ceara, Brazil

[c] Departamento de Física - UNESP - Univ Estadual Paulista - Av. 24A, 1515, 13506-900 - Rio Claro - SP, Brazil

HIGHLIGHTS

- Decay of energy in a dissipative system.
- Corridors created by stable manifolds.
- Theoretical prediction of the energy decay.

ARTICLE INFO

Article history:
Received 25 February 2013
Received in revised form 2 May 2013
Available online 24 May 2013

Keywords:
Fermi map
Decay of energy
Manifolds

ABSTRACT

The behavior of the decay of velocity in a semi-dissipative one-dimensional Fermi accelerator model is considered. Two different kinds of dissipative forces were considered: (i) $F \propto -v$ and; (ii) $F \propto -v^2$. We prove the decay of velocity is linear for (i) and exponential for (ii). During the decay, the particles move along specific *corridors* which are constructed by the borders of the stable manifolds of saddle points. These corridors organize themselves in a very complicated way in the phase space leading the basin of attraction of the sinks to be seemingly of fractal type.

1. Introduction

The one-dimensional Fermi accelerator model was firstly studied by Enrico Fermi who proposed a mechanism to possible explain the acceleration of cosmic rays in the interstellar medium [1]. He assumed that the cosmic particles were accelerated by moving magnetic clouds present in the cosmos. A derivation of this model for a non-relativistic classical particle (representing the cosmic ray) bouncing between walls was then proposed by Ulam [2]. In the model, one wall is moving smoothly and periodically in time, therefore making allusions to the moving magnetic fields, while the other one is considered to be fixed, working as a returning mechanism for the particle to experience a further collision with the moving wall. The model then is known as the Fermi–Ulam model [3–5] and has been studied in many different versions and along several approaches [6–15]. The dynamics of the particle is generally described by a two-dimensional non-linear mapping for the velocity of the particle and time. For periodic oscillations and in the absence of dissipation, the phase space presents a mixed structure in the sense that periodic islands are surrounded by a chaotic sea which is limited by invariant spanning curves. When dissipation is introduced, generally the elliptic islands turn into sinks via a bifurcation. The spanning curves are destroyed and attractors are observed. The model is often used to relate problems involving unlimited energy growth of the bouncing particle, a phenomenon also called Fermi acceleration (FA). Applications of FA have been observed in different

* Corresponding author. Tel.: +55 85 96105335.
E-mail addresses: dftavares@unilab.edu.br (D.F. Tavares), ascanio@fisica.ufc.br (A.D. Araujo), edleonel@rc.unesp.br (E.D. Leonel), rai@fisica.ufc.br, raimundo.costafilho@gmail.com (R.N. Costa Filho).

0378-4371/$ – see front matter © 2013 Elsevier B.V. All rights reserved.
http://dx.doi.org/10.1016/j.physa.2013.05.027

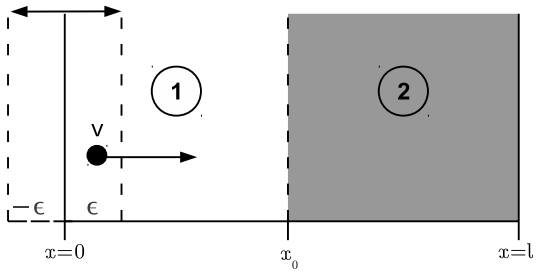

Fig. 1. Sketch of the mixed Fermi accelerator model. Regions 1 and 2 have a different viscous drag force. The equation of the moving wall is given by $x_p(t_n) = \varepsilon \cos(\omega t_n)$.

areas of science including plasma physics [16], astrophysics [17,18], atomic physics [19], optics [20,21] and even in time dependent billiard problems [22]. The phenomenon however seems not to be robust since dissipation is assumed to be a mechanism to suppress Fermi acceleration [23]. The dynamics of particles confined in walls can be used also to describe properties of the so called cavity Optomechanics [24,25], mechanical [26,27] and nano-mechanical resonators [28]. Indeed in such systems, as a influence of the injection of a laser beam, transference of momentum to a mirror (wall) is observed therefore leading to a kind of synchronization of micromechanical [29] or nano-mechanical resonators [30].

In real experiments, dissipation is always present. Therefore one way to consider the presence of damping in the system is to assume that collisions of the particle with the walls are inelastic. It then leads the particle to experience a fractional loss of energy at each collision. The system does not preserve the phase space measure as observed in the non-dissipative case and the mixed structure is changed. In particular, it is possible to observe different asymptotic behavior as the damping coefficient is varied. Among them, effects of transient [31], attractive fixed points [32], chaotic attractors [33], and the occurrence of boundary crisis [34] can all be considered. A different way of introducing dissipation in the system is to consider that the particle is moving along the presence of a viscous drag force, like a fluid. In this paper we consider the effects of a dissipative force of two types [35]: (i) $F \propto -v$ and; (ii) $F \propto -v^2$ where v is the velocity of the particle. The $(-)$ in the expression denotes the force is contrary to the movement of the particle. However, the fluid is not present in the entire accessible region. The distribution of the gas in the system is controlled by a control parameter λ in the sense that for $\lambda = 1$ the system is non-dissipative and for $0 \leq \lambda < 1$ there is a presence of gas in part of the system. Our main goal is to study and characterize the behavior of the velocity of the particle as a function of the number of collisions with the moving wall as well as the control parameters for cases (i) and (ii). As we will show, when the initial velocity is sufficiently high, the particle experiences a decay of velocity which we prove to be: linear for case (i) and exponential for case (ii). Numerical results remarkably give support to our analytical approach. During the decay, we shown that the particle moves in the phase space along specific region we denote as *corridors* whose borders are generated by stable manifolds leaving from a saddle point. These corridors, corresponding to the region delimited by the borders of the stable manifolds, are indeed the basin of attraction of the attractors, mainly the sinks. So far we can tell that this might be the first time that manifolds have been used to defined the corridors' path to describe the decay of energy in such type of systems. Applications to higher dimensional systems are expected to be valid too.

The organization of the paper is as follows. In Section 2 we describe the model and the equations that describe the dynamics for case (i), i.e. when $F \propto -v$. The analytical approach for a decaying particle is constructed and numerical simulations are presented in support of the analytical approach. Section 3 is devoted to discussing the case (ii), $F \propto -v^2$. The decay of velocity is proved to be of exponential type and confirmed by numerical simulations. Our concluding remarks are presented in Section 4.

2. The model, the mapping and results for the case $F \propto -v$

The mixed Fermi accelerator model we are considering here consists of a classical particle of mass m which is confined to bounce between two rigid walls. One of them is fixed and the other one moves periodically in time. The collisions of the particle with either walls are assumed to be elastic. The fixed wall is located at $x = l$ and the moving wall has the equation of the position given by $x_w = \varepsilon \cos(\omega t)$. Here ε is the amplitude of oscillation of the moving wall, ω is the angular frequency and t is time. The region within the interval $x \in [-\varepsilon, \varepsilon]$ is called the collision zone. The velocity of the moving wall is given by $v_w = \mathrm{d}x_w/\mathrm{d}t = -\varepsilon\omega \sin(\omega t)$. We consider the existence of two different regions between the walls, as shown in Fig. 1. Region 1 is given defined by the space between the oscillating wall x_w and the point x_0 while region 2 is given by $x_0 < x \leq l$. It is convenient to introduce the parameter $\lambda = x_0/l$. In the model, we assume that region 1 has no dissipative forces while region 2 has a force like $F = -\eta' v$. The case of $F = -\eta' v^2$ will be considered in Section 3.

As usual in the literature, the dynamics of the model is described by a two dimensional non-linear mapping for the variables (v, t), where v and t are respectively the particle's velocity after the collision with the moving wall and the time at the collision. When moving in the viscous region, the particle is experiencing continuously a reduction of its velocity. The mapping T is given by $T(v_n, t_n) = (v_{n+1}, t_{n+1})$ where the index denotes respectively collisions nth and $(n+1)$th. To construct the mapping and to avoid privileging any initial condition, we assume that at the instant $t = t_n > 0$, the particle is in the position $x_p(t_n) = \varepsilon \cos(\omega t_n)$ with velocity $v = v_n$. Such a choice is made because it corresponds indeed to the

evolution of an ongoing orbit. The Newton's Second Law, $\sum F = ma$, completely describes the solution of the problem, specifying the velocity and position of the particle at a given instant. While in region 1 the velocity is constant, in region 2 we have to solve

$$-\eta' v = m\frac{dv}{dt}. \tag{1}$$

To find the velocity at any time in region 2 we integrate the above equation leading to

$$v_p(t) = \begin{cases} v_n, & -\varepsilon < x \le x_0 \\ v_n \exp(-\eta(t - t_{r_1})), & x_0 < x \le l, \end{cases} \tag{2}$$

for $t \ge t_{r_1}$, where t_{r_1} is the time spent by the particle traveling in region 1 to the right. Here we define $\eta = \eta'/m$. To find the position of the particle when it moves to the right we have

$$x_p(t) = \begin{cases} \varepsilon\cos(\omega t_n) + v_n(t - t_n) & \text{for region 1} \\ \varepsilon\cos(\omega t_n) + v_n t_{r_1} + v_n[1 - \exp(-\eta(t' - t_{r_1}))], & \text{for region 2,} \end{cases} \tag{3}$$

with $t \ge t_n$ and $t' \ge t_{r_1}$. Considering elastic collisions with both walls and defining a set of dimensionless and therefore more convenient variables $V_{n+1} = (v_{n+1}/\omega l)$, $\phi_{n+1} = (\omega t_{n+1})$, $\epsilon = (\varepsilon/l)$ we find that the mapping is given by

$$T : \begin{cases} V_{n+1} = V_n{}^* - 2\epsilon\sin(\phi_{n+1}) \\ \phi_{n+1} = [\phi_n + \Delta T_n] \mod (2\pi), \end{cases} \tag{4}$$

where the expressions for $V_n{}^\star$ and ΔT_n are given according to the type of collision, namely: (a) multiple – those happening with the moving wall before the particle leaves the collision zone or; (b) indirect collisions – those where the particle hits one wall and in sequence it hits the opposite wall.

For multiple collisions the particle collides more than once with the moving wall before leaving the collision zone. Then, $V_n{}^* = -V_n$ e $\Delta T_n = \phi_c$, where ϕ_c is obtained by the smallest solution of the transcendental equation

$$G(\phi_c) = \epsilon[\cos(\phi_{n+1}) - \cos(\phi_n)] - V_n\phi_c = 0, \tag{5}$$

with $\phi_c \in (0, 2\pi]$. For the non-dissipative case, the phase space preserves the measure $\mathrm{d}\mu = (V + \epsilon\sin(\phi))dVd\phi$. For applications in a non-dissipative model see Ref. [36]. Our results considering multiple collisions produce a determinant of the Jacobian matrix given by

$$\det(J_{MC}) = \frac{V_n + \epsilon\sin(\phi_n)}{V_{n+1} + \epsilon\sin(\phi_{n+1})}, \tag{6}$$

which is the same as the conservative case.

On the other hand when indirect collisions are considered, the particle collides once with the moving wall and leaves the collision zone. However in this mixed model, the particle travels in two different regions with different viscous drag force. Therefore, we obtain $V_n^* = -V_m$, where $V_m = -[V_n - 2\delta(1-\lambda)]$ and $\Delta T_n = \phi_{r_1} + \phi_T + \phi_{l_1} + \phi_c$. The auxiliary terms ϕ_{r_1}, ϕ_T and ϕ_{l_1} are given by

$$\begin{aligned} \phi_{r_1} &= \frac{\lambda - \epsilon\cos(\phi_n)}{V_n}, \\ \phi_{l_1} &= \frac{\lambda - \epsilon}{V_n}, \\ \phi_T &= -\frac{1}{\delta}\ln\left[1 - \frac{2\delta(1-\lambda)}{V_n}\right]. \end{aligned} \tag{7}$$

The term ϕ_{r_1} refers to the time the particle traveled to the right in region 1, ϕ_T is total time spent in region 2, and ϕ_{l_1} is the time the particle takes to travel in region 1 again to the left. The term ϕ_c is obtained from $F(\phi_c) = 0$, where

$$F(\phi_c) = \epsilon\cos(\phi_{n+1}) - \epsilon - V_m\phi_c = 0, \tag{8}$$

with $\phi_c \in [0, 2\pi]$, $\delta = \eta/\omega$, and $\lambda = x/l$.

The determinant of the Jacobian matrix for the case of indirect collisions gives us that

$$\det(J_{IC}) = -\frac{V_m}{V_n}\frac{V_n + \epsilon\sin(\phi_n)}{V_{n+1} + \epsilon\sin(\phi_{n+1})}. \tag{9}$$

The fraction V_m/V_n approaches unity when $\lambda \to 1$, therefore recovering the non-dissipative case.

The presence of dissipation leads the dynamics to exhibit attractors. For large finite velocities an exponential decay of the velocity magnitude is expected to be observed, therefore converging to the attractors. We indeed observe this behavior.

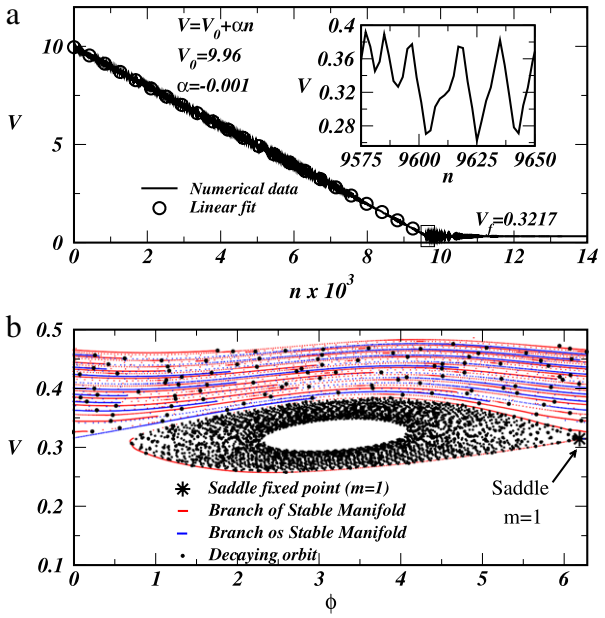

Fig. 2. (a) Plot of V against n for the parameters $\delta = 10^{-3}$, $\epsilon = 10^{-2}$ and $\lambda = 0.5$. The initial condition used was $(V_0, \phi_0) = (10, 1)$. The zoom in shows the behavior of V near a passage to a period one zone of attraction. The final convergence of V is $V_f = 0.3217\ldots$. (b) Plot of V as a function of ϕ for the same parameters of (a). The decay of V happens in a specific region delimited by two branches of the stable manifold (blue and red curves) of a period one saddle fixed point, which we call a corridor. (For interpretation of the references to colour in this figure legend, the reader is referred to the web version of this article.)

To have an idea of the type of decay, let us compose the equation of the velocity in the mapping (4) a few times. So starting with V_0 we obtain firstly

$$V_1 = V_0 - 2\delta(1-\lambda) - 2\epsilon \sin(\phi_1) \tag{10}$$

iterating in sequence we obtain

$$V_2 = V_0 - 4\delta(1-\lambda) - 2\epsilon \sin(\phi_1) - 2\epsilon \sin(\phi_2), \tag{11}$$

and

$$V_3 = V_0 - 6\delta(1-\lambda) - 2\epsilon \sin(\phi_1) - 2\epsilon \sin(\phi_2) - 2\epsilon \sin(\phi_3), \tag{12}$$

which allows us to obtain the general decay relation as

$$V_n = V_0 - 2n\delta(1-\lambda) - 2\epsilon \sum_{i=1}^{n} \sin(\phi_i). \tag{13}$$

If we assume that $V_0 \gg \epsilon$, say $V_0 = 10^3\epsilon$, the sum on the right hand side can be neglected therefore leading us to conclude that

$$V_n = V_0 - 2n\delta(1-\lambda). \tag{14}$$

Fig. 2(a) shows the behavior of the velocity of the particle as a function of the number of collisions with the boundary for the control parameters: $\epsilon = 10^{-2}$, $\lambda = 0.5$, $\delta = 10^{-3}$ and considering $V_0 = 10 = 1000\epsilon$. A linear fitting furnishes a slope -0.001 in total agreement with Eq. (14). The initial condition used was $(V_0, \phi_0) = (10, 1)$. To solve numerically Eqs. (5) and (8) we used the so called bisection method considering the solution inside an accuracy of 10^{-12}. The plot shown in Fig. 2(a) shows a linear decay for short n when the curve bends towards a regime of convergence reaching a constant plateau at velocity $V_f = 0.3217\ldots$ for sufficiently large n. This plateau corresponds to the velocity of a period one sink fixed point. Indeed, to obtain the fixed points, we have to solve simultaneously the following conditions: $V_{n+1} = V_n$ and $\phi_{n+1} = \phi_n + 2m\pi$ and $m = 1, 2, 3, \ldots$. Such conditions give rise to two sets of fixed points:

$$(V_1, \phi_1) = \left(V_1, \arcsin\left[-\frac{\delta}{\epsilon}(1-\lambda)\right]\right), \tag{15}$$

and

$$(V_2, \phi_2) = \left(V_2, \pi - \arcsin\left[-\frac{\delta}{\epsilon}(1-\lambda)\right]\right), \tag{16}$$

Table 1
Table showing ϵ and the largest m for which the fixed point (16) is a sink. The parameters used were $\delta = 10^{-3}$ and $\lambda = 0.1$.

ϵ	Larger m to have Eq. (16) a sink
0.01	3
0.02	2
0.03	1
0.04	1
0.05	1

Table 2
Table showing ϵ and the largest m for which fixed point (16) is a sink. The parameters used were $\delta = 10^{-4}$ and $\lambda = 0.1$.

ϵ	Larger m to have Eq. (16) a sink
1×10^{-3}	15
2×10^{-3}	7
3×10^{-3}	6
4×10^{-3}	5
5×10^{-3}	4
6×10^{-3}	4
7×10^{-3}	3
8×10^{-3}	3
9×10^{-3}	3

Table 3
Table showing ϵ and the largest m for which fixed point (16) is a sink. The parameters used were $\delta = 10^{-3}$ and $\lambda = 0.5$.

ϵ	Larger m to have Eq. (16) a sink
6×10^{-4}	8
7×10^{-4}	8
8×10^{-4}	7
9×10^{-4}	7
1×10^{-3}	7
2×10^{-3}	6
3×10^{-3}	6
4×10^{-3}	5
5×10^{-3}	5
6×10^{-3}	5
7×10^{-3}	5
8×10^{-3}	5
9×10^{-3}	5

where V_i with $i = 1, 2$ are the numerical solutions obtained from $K(V_i) = 0$, where

$$K(V_i) = \frac{2V_i(\lambda - \epsilon\cos(\phi_i))}{V_i(V_i - 2\delta(1-\lambda))} + \frac{2\delta(1-\lambda)(\epsilon + \epsilon\cos(\phi_i) - 2\lambda)}{V_i(V_i - 2\delta(1-\lambda))} - 2m\pi - \frac{1}{\delta}\ln\left[1 - \frac{2\delta(1-\lambda)}{V_i}\right]. \tag{17}$$

From Eqs. (15) and (16) we can conclude that the fixed points exist only if the condition $\delta(1-\lambda) \leq \epsilon$ is matched. The stability of the fixed points can also be investigated. Considering we have three relevant control parameters, namely, ϵ, δ and λ and taking into account that the velocity of the fixed point can only be obtained from numerical solution of Eq. (17), an analytical result for the stability of fixed points become almost impossible. However we have considered separate sets of control parameters and investigate the stability of the fixed points. For specific discussions see Ref. [37]. Let us start with a fixed $\delta = 10^{-3}$ and $\lambda = 0.1$. Table 1 shows the corresponding ϵ and the largest m for which the fixed point given by Eq. (16) is a sink. For this set of control parameters, fixed point (15) is a saddle.

Considering now the set of control parameters $\delta = 10^{-4}$ and $\lambda = 0.1$, the conditions to make Eq. (16) a sink are shown in Table 2.

Considering a different parameter $\lambda = 0.5$ and fixing $\delta = 10^{-3}$, the conditions to make Eq. (16) a sink are shown in Table 3.

If we consider now a set of $\delta = 10^{-3}, \epsilon = 10^{-3}$ and let λ vary, eventually fixed point (16) bifurcates from sink to saddle. However the opposite may also happen, i.e., fixed point (15) may bifurcate from saddle to sink and to saddle again as m varies. Table 4 shows the corresponding values of λ and m that makes Eq. (16) a sink (column 2) and Eq. (15) a sink (column 3).

Table 4
Table showing λ and the largest m for which fixed point (16) is a sink (column 2) and the corresponding range of m for which fixed point (15) is a sink (column 3). The parameters used were $\delta = 10^{-3}$ and $\epsilon = 10^{-3}$.

ϵ	Larger m—Eq. (16)	Range of m—Eq. (15)
0.1	7	8–10
0.2	5	6–8
0.3	5	6–7
0.4	5	6–7
0.5	5	6–7
0.6	5	6–7
0.7	5	6–7
0.8	5	6–8
0.9	7	8–9

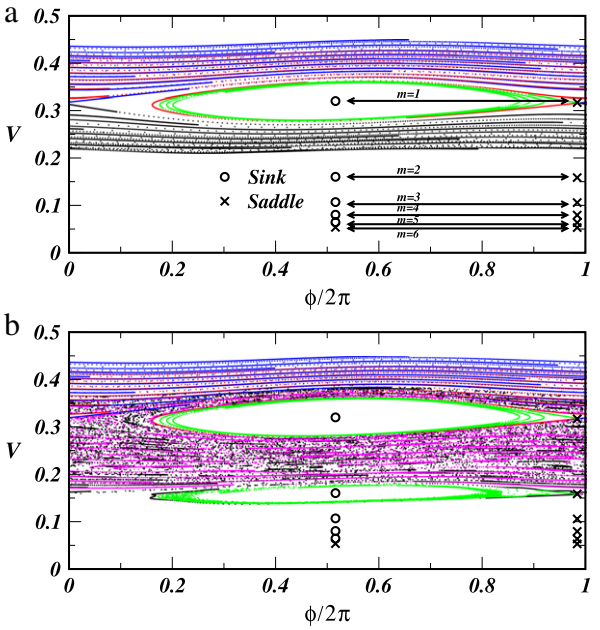

Fig. 3. (a) Plot of the stable and unstable manifolds for a saddle fixed point with $m = 1$. The control parameters used were $\delta = 10^{-3}$, $\epsilon = 5 \times 10^{-3}$ and $\lambda = 0.5$. The two branches of the stable manifold define the borders of the corridor. (b) Stable manifolds for saddle given by Eq. (15) with $m = 1$ and $m = 2$ and one of the unstable manifolds spiraling to the sinks.

Given the sinks are now known for a variety of set of control parameters, let us now discuss more specifically the way the particle evolves in the phase space along its decaying of velocity. Indeed for the present model, the particle moves along specific *corridors* that are created by the basin of attraction of the sinks. Additionally, for a fixed m, the basin of attraction is constrained by the two branches of the stable manifold of a saddle fixed point that characterizes the sink (see Eqs. (15) and (16)). An example of this decay is shown in Fig. 2(b) where the red and blue curves correspond to the corridor formed by the border of the two stable manifolds. The stable manifolds are obtained by iterating the inverse of the mapping T given by Eq. (4). Therefore T^{-1} is given by

$$T^{-1}: \begin{cases} V_n = V_{n+1} + 2\delta(1-\lambda) + 2\epsilon \sin(\phi_{n+1}) \\ \phi_n = \left[\phi_{n+1} - \left(\dfrac{\lambda - \epsilon\cos(\phi_n)}{V_n}\right) - \dfrac{\lambda-\epsilon}{V_n}\right] + \dfrac{1}{\delta}\ln\left[1 - \dfrac{2\delta(1-\lambda)}{V_n}\right] \\ \qquad - \left[\dfrac{\epsilon - \epsilon\cos(\phi_{n+1})}{V_n - 2\delta(1-\lambda)}\right] \mod(2\pi). \end{cases} \tag{18}$$

The solution for ϕ_n is obtained numerically from the second equation of mapping (18) with an accuracy of 10^{-12}. Indeed the organization of the manifolds is as follows. Two branches are stable, obtained from mapping (18) and two of them are unstable. The latter is obtained by iterating mapping (4).

Fig. 3(a) shows the corresponding plot of the four branches of saddle fixed point obtained for $m = 1$ from Eq. (15) for the parameters $\delta = 10^{-3}$, $\epsilon = 5 \times 10^{-3}$ and $\lambda = 0.5$. The red and blue lines correspond to the stable manifolds and define the borders of the corridor through which the particles move coming from high energy (if the initial condition is given at such

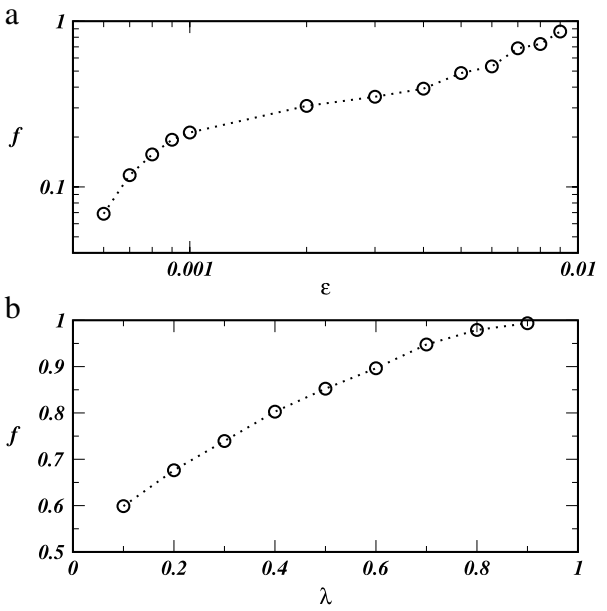

Fig. 4. Plot of the fraction of orbits trapped by sinks considering a grid of 10^6 initial conditions for the parameters $\delta = 10^{-3}$ and: (a) $\lambda = 0.5$ and; (b) $\epsilon = 10^{-2}$.

corridor). The green curve is one of the unstable branch and it converges towards the sink making spirals while the black curve is the second unstable branch and moves downwards the velocity axis. Eventually it can cross the basin of attraction of lower sinks and be captured for one of them for sufficiently long time. Black bullets denote the sinks while the red crosses correspond to the saddle point. For the set of control parameters chosen, the fixed point (16) becomes a saddle for $m = 6$, as is shown in the plot. As the curves of the stable manifolds move upward on the velocity axis, they become close to each other making the corridor where the particle moves thinner and thinner. The same scenario is observed for the manifolds of a saddle point obtained for $m = 2$, as is shown in Fig. 3(b). We see that the corridor, now marked by the borders in light blue and magenta, are thinner than that observed for $m = 1$. The spirals moving towards the sink are now more evident for the unstable manifolds leaving saddle for $m = 2$. One can also see that the corridor for the sink in $m = 1$ is still untouched by the one generated for $m = 2$. The same procedure is observed for other values of m. However, the complexity of these curves making the borders for the basin of attraction for the sinks become very high and that the investigation following this procedure becomes impossible. When the particle acquires low velocity it may have a chance of wander in a chaotic way in the phase space until being captured by a sink or it may, eventually, have all of its energy dissipated by the drag force. This situation leads the particle to reach the state of rest, therefore stopping between the two walls. To have an idea of the amount of particles that stop their dynamics having all energy dissipated by the drag force, we evolved a grid of initial conditions in the phase space and followed each one of them in time to obtain the asymptotic behavior. Therefore two things may occur: (1) the particles are trapped by the attractors or; (2) they have their energy totally dissipated. To conduct the simulations, we considered 1000 initial phases $\phi_0 \in (0, 2\pi]$ and 1000 different velocities $V_0 \in (2\epsilon, 0.4]$, therefore leading to an ensemble of 10^6 different initial conditions. Each particle was left to evolve until 10^5 collisions with the moving wall. At the end, the fraction of particles that have their energy dissipated was accounted.

Fig. 4 shows the corresponding plot of the fraction of particles that survive the dissipation, i.e., are trapped by sinks as function of: (a) the parameter ϵ for a fixed $\delta = 10^{-3}$ and $\lambda = 0.5$ and; (b) the parameter λ for a fixed $\delta = 10^{-3}$ and $\epsilon = 10^{-2}$. To illustrate in the phase space the fraction of particles that survive the dissipation, we show in Fig. 5 a plot of the initial conditions V vs. ϕ that are trapped by sinks. We use the same figure to show the corridors appearing from the stable manifolds generated for the saddles given by Eqs. (15) and (16) considering $m = 1$ and $m = 2$. Other corridors also exist but they are too thin to be shown in the plot. The gray color denotes the initial conditions that survive the dissipation.

Considering that the trapping mechanism is now understood, let us now discuss the behavior of the decay as a function of the control parameters. Fig. 6(a) shows a plot of the decaying velocity for three different values of the control parameter, namely: $\lambda = 0$ (total space is filled by gas), $\lambda = 0.5$ and $\lambda = 1$ (non-dissipative). Fig. 6(b) shows the corresponding slope of the decay as function of the control parameter λ. The results presented in Fig. 6 are in total agreement with the theoretical prediction given by Eq. (14).

3. The mapping and results for the case $F \propto -v^2$

Let us now consider the case (ii), i.e., the force acting on the particle is of the type $F \propto -v^2$. The dynamics of the particle is given by a two-dimensional mapping for the same set of variables and dimensionless control parameters as discussed in the

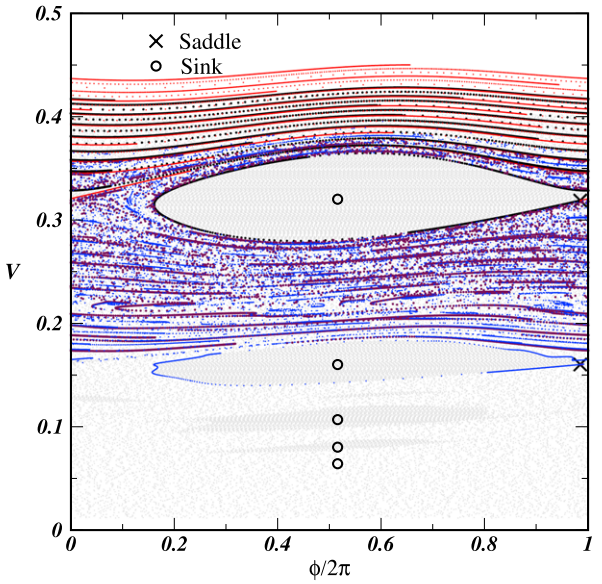

Fig. 5. Plot of the initial conditions in the plane V against ϕ that are trapped by the attractors (gray color). The control parameters are $\delta = 10^{-3}$, $\epsilon = 5 \times 10^{-3}$ and $\lambda = 0.5$. Black bullets denote the period-one sinks. Corridors are constructed by the stable manifolds of the saddle points.

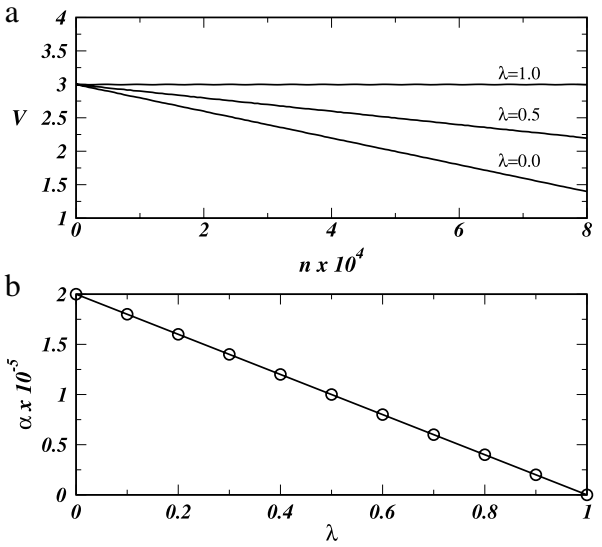

Fig. 6. (a) Plot of V against n for different values of the parameter λ. (b) The slope of the curves as a function of λ.

previous section. Therefore mapping (4) describes well the dynamics of the particle. For the case where the particle moves in the absence of dissipation, the dynamics is totally described by the same set of equations as in the previous section. The change happens when the particle moves along the damping region. Therefore and after solving Newton's law of motion, the indirect collisions are given by $V_n{}^* = -V_m$, where

$$V_m = -\frac{V_n}{e^{2\delta(1-\lambda)}},$$

and $\Delta T_n = \phi_{r_1} + \phi_T + \phi_{l_1} + \phi_c$. The auxiliary variables ϕ_{r_1}, ϕ_T and ϕ_{l_1} are given by

$$\phi_{r_1} = \frac{\lambda - \epsilon\cos(\phi_n)}{V_n}, \qquad \phi_{l_1} = \frac{\lambda - \epsilon}{V_n}, \qquad \phi_T = \frac{e^{2\delta(1-\lambda)} - 1}{V_n\delta}, \tag{19}$$

and $\phi_c \in [0, 2\pi)$ is numerically obtained by equaling the position of the particle and the moving wall, which corresponds to the same Eq. (8). The Jacobian recovers the same expression as in the previous with the proper expression for V_m.

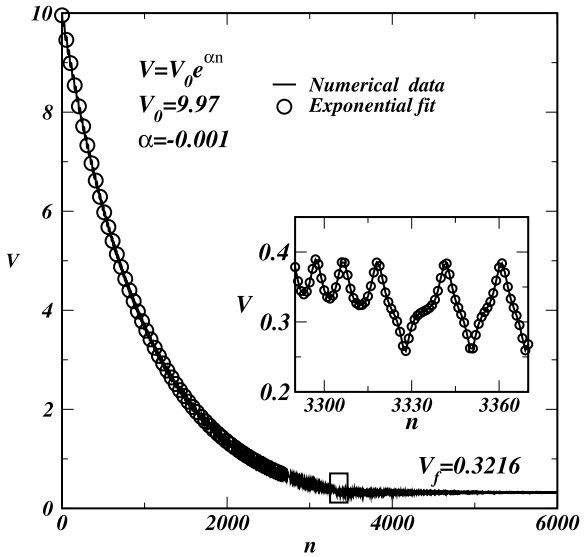

Fig. 7. Plot of V against n for the parameters $\delta = 10^{-3}$, $\epsilon = 10^{-2}$ and $\lambda = 0.5$. The initial condition used was $(V_0, \phi_0) = (10, 1)$. The zoom in shows the behavior of V near a passage to a period one zone of attraction. The final convergence of V is $V_f = 0.3216\ldots$.

Let us start the investigation with the decay of velocity. To do so, we compose the equation of the velocity from mapping (4). Therefore we have

$$V_1 = \frac{V_0}{\exp(2\delta(1-\lambda))} - 2\epsilon \sin(\phi_1), \tag{20}$$

and a second composition gives

$$V_2 = \frac{V_0}{\exp(2(2\delta(1-\lambda)))} - \frac{2\epsilon \sin(\phi_1)}{\exp(2\delta(1-\lambda))} - 2\epsilon \sin(\phi_2), \tag{21}$$

and

$$V_3 = \frac{V_0}{\exp(3(2\delta(1-\lambda)))} - \frac{2\epsilon \sin(\phi_1)}{\exp(2(2\delta(1-\lambda)))} - \frac{2\epsilon \sin(\phi_2)}{\exp(2\delta(1-\lambda))} - 2\epsilon \sin(\phi_3). \tag{22}$$

After a generalization we end up with the relation

$$V_n = \frac{V_0}{\exp(n2\delta(1-\lambda))} - 2\epsilon \sum_{i=1}^{n} \frac{\sin(\phi_i)}{\exp((n-\mathrm{i})2\delta(1-\lambda))}. \tag{23}$$

Considering again that the initial velocity is sufficiently large, say $V_0 = 1000\epsilon$, the second term in Eq. (23) is negligible, therefore the main term in the decay is given by

$$V_n = \frac{V_0}{\exp(n2\delta(1-\lambda))}. \tag{24}$$

Our numerical results remarkably recovers well the theoretical prediction. It is shown in Fig. 7 the corresponding decay of velocity for the control parameters $\delta = 10^{-3}$, $\epsilon = 10^{-2}$ and $\lambda = 0.5$.

The convergence to the constant plateau is explained as in the previous section. Indeed the particle is evolving along the basin of attraction of a period-one sink ($m = 1$). The decay of the velocity in the phase space also occurs along the corridor generated by the stable manifolds which produce the borders of the basin of attraction. The difference in this section is that the particle does not have its energy entirely dissipated by the damping force. Consequently, as the velocity of the particle reduces, the force acting on it reduces too, letting the particle have a chance of experiencing a further collision with the moving wall and raising the velocity until finding its final state at an attractor.

Extensive numerical simulations were made for different values of λ and all simulations confirm our theoretical prediction. Fig. 8(a) shows the exponential decay for the velocity considering three different values of λ, as labeled in the figure. For the case of $\lambda = 1$ a constant plateau is observed, as expected since in that regime the model is purely conservative. Moreover, the decay is numerically fitted by $V(n, \lambda) = 3\exp[-A(\lambda)n]$, where the parameter $A(\lambda) = 2(1-\lambda)$, in total agreement with Eq. (23). The slope of the decay is shown in Fig. 8(b) for a large range of λ.

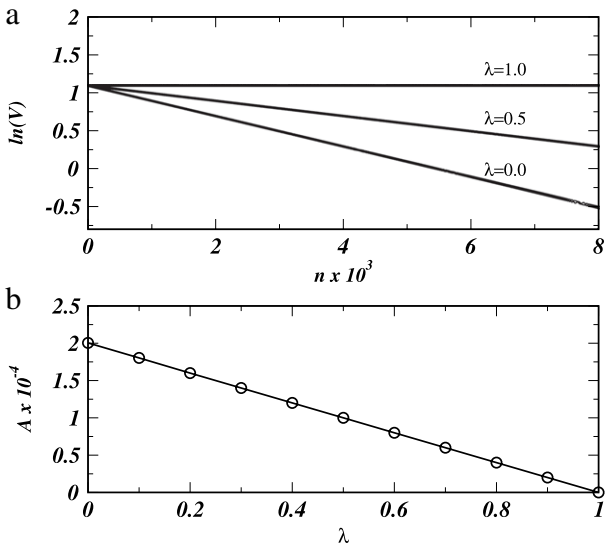

Fig. 8. (a) Plot of V against n for different values of the parameter λ. (b) The slope of the curves as a function of λ.

4. Conclusions

In summary, we have considered some dynamical properties for a mixed Fermi accelerator model. In this model the space between the walls is divided in two different regions. One where the particle does not experience any dissipative force and another one where a dissipative force is present. A dimensionless parameter was introduced in order to control the size of the dissipative/non-dissipative region. In both studied cases, we noticed that the velocity of the particle decreases and it decays smoothly as the conservative region starts to be dominant. We prove that the decay of the velocity is linear for case (i) and exponential for case (ii). Numerical results support the theoretical approach. During the decay, the particle moves along corridors created by the stable manifolds of saddle points. Therefore we developed a systematic method to study the simplest one-dimensional case but with several possibilities where a particle can cross different fluid regions with different viscosity or drag force.

In terms of a possible connection with an experiment, we can suppose that there are two linear cavities connected by a hole. One cavity is at high temperature where thermal vibrations work like a perturbation to the boundary given (in the average) energy to the particle upon collisions. The other cavity is at low temperature and filled with gas to where the particle must cross losing energy along the trajectory. The ratio of the lengths of the two cavities controls the damping term. Changing a gas filling the cavity, let us say, by a much more dense one, drag force is changed therefore controlling also the drag coefficient. The dynamics of the particles in such a system can be described, at first approach, by the model discussed in this paper.

As a perspective of the study one can consider the dynamics of interacting particles (via collision for example) in the system therefore leading to a possible synchronization of motions. Due to the presence of the dissipation, the particles may reach different steady states, characterized by different attractors in the phase space. As the dissipation is varied, the steady states may change from stable to unstable (fixed points of sink type). Additionally, the decay of energy should depend on the shape of the manifolds. As the system is now composed by more than one particle, such manifolds may have extremely complicated forms.

Acknowledgments

DFT, ADA and RNCF thanks Conselho Nacional de Desenvolvimento Científico e Tecnológico—CNPq, Brazilian agency. EDL acknowledges the financial support by FAPESP, CNPq and FUNDUNESP, Brazilian agencies. This research was supported by resources supplied by the Center for Scientific Computing (NCC/GridUNESP) of the São Paulo State University (UNESP).

References

[1] E. Fermi, Phys. Rev. 75 (1949) 1169.
[2] S. Ulam, Proc. 4th Berkeley Symposium on Math, Statistics and Probability, Vol. 3, California University Press, Berkeley CA, 1961, p. 315.
[3] M.A. Lieberman, A.J. Lichtenberg, Phys. Rev. A 5 (1972) 1852.
[4] L.D. Pustylnikov, Dokl. Akad. Nauk SSSR 241 (1978) 1035.
[5] L.D. Pustylnikov, Sov. Math. Dokl. 35 (1987) 1.
[6] S.T. Dembinski, A.J. Makowski, P. Peplowski, Phys. Rev. Lett. 70 (1993) 1093.

[7] J.V. José, R. Cordery, Phys. Rev. Lett. 56 (1986) 290.
[8] M.E. Flatte', M. Holthaus, Ann. Phys., NY 245 (1996) 113.
[9] F. Saif, I. Rehman, Phys. Rev. A 75 (2007) 043610.
[10] R.M. Everson, Physica D 19 (1986) 355.
[11] P.J. Holmes, J. Sound Vib. 84 (1982) 173.
[12] Z.J. Kowalik, M. Franaszek, P. Pieranski, Phys. Rev. A 37 (1988) 4016.
[13] S. Warr, W. Cooke, R.C. Ball, J.M. Huntley, Physica A 231 (1996) 551.
[14] L. Matyas, R. Klages, Physica D 187 (2004) 165.
[15] A. Mehta, J.M. Luck, Phys. Rev. Lett. 65 (1990) 393.
[16] A.V. Milovanov, L.M. Zelenyi, Phys. Rev. E 64 (2001) 052101.
[17] A. Veltri, V. Carbone, Phys. Rev. Lett. 92 (2004) 143901.
[18] K. Kobayakawa, Y.S. Honda, T. Samura, Phys. Rev. D 66 (2002) 083004.
[19] G. Lanzano, et al., Phys. Rev. Lett. 83 (1999) 4518.
[20] F. Saif, I. Bialynicki-Birula, M. Fortunato, W.P. Schleich, Phys. Rev. A 58 (1998) 4779.
[21] A. Steane, P. Szriftgiser, P. Desbiolles, J. Dalibard, Phys. Rev. Lett. 74 (1995) 4972.
[22] A. Loskutov, A.B. Ryabov, J. Stat. Phys. 108 (2002) 995.
[23] E.D. Leonel, J. Phys. A 40 (2007) F1077.
[24] T.J. Kippenberg, K.J. Vahala, Science 321 (2008) 172.
[25] F. Marquardt, S.M. Girvin, Physics 2 (2009) 40.
[26] A. Schliesser, O. Arcizet, R. Riviere, G. Anetsberger, T.J. Kippenberg, Nat. Phys. 5 (2009) 509.
[27] R. Riviere, et al., Phys. Rev. A 83 (2011) 063835.
[28] M. Bagheri, M. Poot, M. Li, W.P.H. Pernice, H.X. Tang, Nat. Nanotechnol. 6 (2011) 726.
[29] M. Zhang, et al. 04 June 2012. arXiv:1112.3636v2 [physics.optics].
[30] C.A. Holmes, C.P. Meaney, G.J. Milburn, Phys. Rev. E 85 (2012) 066203.
[31] M.A. Lieberman, K.Y. Tsang, Phys. Rev. Lett. 55 (1985) 908.
[32] J.M. Luck, A. Mehta, Phys. Rev. E 48 (1993) 3988.
[33] K.Y. Tsang, M.A. Lieberman, Physica D 11 (1984) 147.
[34] E.D. Leonel, P.V.E. McClintock, J. Phys. A 38 (2005) L425.
[35] D.F. Tavares, E.D. Leonel, R.N. Costa Filho, Physica A 391 (2012) 5366.
[36] E.D. Leonel, P.V.E. McClintock, J. Phys. A 38 (2005) 823.
[37] A.J. Lichtenberg, A.M. Lieberman, Regular and Chaotic Dynamics, in: Applied Mathematical Sciences, vol. 38, Springer, New York, 1992.